

Electronically modulated two-dimensional plasmons coupled to surface plasmon modes

Godfrey Gumbs

Department of Physics and Astronomy, Hunter College of the City University of New York, 695 Park Avenue, New York, New York 10021, USA

Danhong Huang

Air Force Research Laboratory (AFRL/VSSS), Kirtland Air Force Base, New Mexico 87117, USA

(Received 14 November 2006; published 12 March 2007)

We present a calculation for a two-dimensional (2D) electron gas layer interacting with a slab of conductive material. We treat the plasmons in the slab in the local limit and obtain the frequency of the coupled mode corresponding to the extended 2D plasmon interacting with the background plasmons in the presence of a conducting surface. The dispersion equation of a double quantum well is obtained and we show how the split symmetric and antisymmetric modes are formed and modified by the localized surface plasmon. For a single layer, we show that when a one-dimensional (1D) periodic electrostatic potential is applied to the surface, each of the symmetric and antisymmetric modes will be further split by the interaction with the 1D modulation, leading to folding of plasmon dispersion curves for different modes. For double layers, we show that the coupled 2D and surface plasmons may result in radiated energy. Our analysis is based on a calculation of the surface response function obtained using a transfer-matrix method.

DOI: [10.1103/PhysRevB.75.115314](https://doi.org/10.1103/PhysRevB.75.115314)

PACS number(s): 71.45.Gm, 73.20.Mf, 34.50.Bw

I. INTRODUCTION

It is well known that for a pair of coupled layers of two-dimensional electron gas (2DEG), the plasmon modes may radiate energy.¹⁻¹² The current research which is being actively pursued, involving a double-quantum-well structure with a grating gate, is concerned with investigating whether the terahertz radiation by the plasmon modes could be employed in electronically tunable detectors.^{5,12-16} The spectral bandwidths of these grating-gated field-effect transistors are of the order of 50 GHz. This range of frequency has proven useful in developing highly sensitive detectors and sensors. van Zyl and Zaremba¹² have studied the behavior of the collective plasma excitations of a 2DEG in the presence of an arbitrary lateral electrostatic modulation. Furthermore, recent experiments have shown that the two-dimensional (2D) plasmon modes of high-mobility grating-gated field-effect transistors could be excited and could be at resonance with the incident terahertz radiation. Besides modulating the electron density at a specific wave vector, the grating gate induces a longitudinal modulation of the incident radiation. As a result of both these effects, the incident radiation is polarized perpendicular to the grating lines to excite and be absorbed by 2D plasmons at the wave vector specified by the grating gate. In this paper, we have demonstrated that when a periodic electrostatic potential is applied to a conducting surface supporting a 2DEG, the coupling between the 2D and three-dimensional (3D) surface plasmons can result in radiated energy from the plasmon excitations. The bulk material must be adequately doped for effective coupling between the collective excitations.

Here, we calculate the effect which a periodic electrostatic modulation has on the coupled 2D plasmon modes. The 2D sheet of electrons interacts with an adjoining slab of conductive material, which could be heavily doped so as to enhance the coupling between the 2D plasmon and 3D surface plasmon. The formalism which we use is based on the surface

response function which appears in the power absorption spectrum when electrons in the medium are excited by an external electromagnetic field.

Early theoretical research done by the Mills and Maradudin¹⁷ and experimental researches done by Moreland *et al.*¹⁸ and Tsang *et al.*¹⁹ all dealt with scattering of the near field associated with the surface-plasmon-polariton (SPP) to the radiation of the far field related to the so-called radiation loss of SPP. This scattering process requires the presence of some surface structures, e.g., surface roughness or a grating, to satisfy momentum conservation. In this case, both the near field and far field are transverse electromagnetic fields. However, in our current study, we only concentrate on the modes of longitudinal electromagnetic fields connected to induced plasma waves in the nonretardation limit. These modes are generally determined by zeros of the determinant of a dielectric-function matrix, as we obtain below.

The main results of our calculations are summarized as follows. We have demonstrated that when a periodic electrostatic potential is applied to a conducting surface supporting a 2DEG, the coupling between the 2D plasmon and 3D surface plasmon can result in a gain or loss in energy from the plasmon excitations when an incident beam of charged particles (a current) impinges on the structure. The bulk material must be adequately doped for effective coupling between the collective excitations. The effect due to a periodic modulation on the plasmons in a biplane is calculated. We obtain the plasmon dispersion relation in this case, as well as the loss function associated with these collective excitations. The presence of the one-dimensional (1D) modulation is found to enhance either a gain or a loss in energy of the incident beam of charged particles.

The paper is organized as follows. We will first describe in Sec. II the formalism for the power absorption in terms of the surface response function.²⁰⁻²⁸ In Sec. III, we explicitly calculate the surface response function for a double quantum well, which we model as a pair of parallel 2D layers of

electron gas (EG). This method allows us to include the coupling between the background 3D electron gas with the 2DEG layers. The dispersion equation we obtain is well known. However, we are able to extend our calculation to include the effects due to an electrostatic modulation on the surface. We also present and discuss the results of our numerical calculations in Sec. IV and concluding remarks in Sec. V.

II. ENERGY LOSS AND THE SURFACE RESPONSE FUNCTION

The subject of electron energy loss has received a considerable amount of attention over the years, with several review articles and books written in the last few years.²⁹ Here, we give a formalism in terms of the surface response function $g(q_{\parallel}, \omega)$. Let us assume that the medium occupies the half-space $z > 0$. Consider a point charge Ze moving along a prescribed trajectory $\mathbf{r}(t)$ outside the medium. The external potential ϕ_{ext} satisfies Poisson's equation in the nonretarded limit:³⁰

$$\nabla^2 \phi_{\text{ext}}(\mathbf{r}, t) = 4\pi Ze \delta[\mathbf{r} - \mathbf{r}(t)]. \quad (1)$$

We now write down the solution of this equation in the region of interest, i.e., $0 > z > z(t)$, with

$$\phi_{\text{ext}}(\mathbf{r}, t) = \int d^2 \mathbf{q}_{\parallel} \int_{-\infty}^{\infty} d\omega \tilde{\phi}_{\text{ext}}(\mathbf{q}_{\parallel}, \omega) e^{i(\mathbf{q}_{\parallel} \cdot \mathbf{r}_{\parallel} - \omega t)} e^{q_{\parallel} z}, \quad (2)$$

where

$$\tilde{\phi}_{\text{ext}}(\mathbf{q}_{\parallel}, \omega) = -\frac{Ze}{4\pi^2 q_{\parallel}} F(\mathbf{q}_{\parallel}, \omega), \quad (3)$$

with

$$F(\mathbf{q}_{\parallel}, \omega) \equiv \int_{-\infty}^{\infty} dt e^{-q_{\parallel} z(t)} e^{i[\omega t - \mathbf{q}_{\parallel} \cdot \mathbf{x}_{\parallel}(t)]}. \quad (4)$$

Here, $\mathbf{q}_{\parallel} = (q_x, q_y)$ is a two-dimensional wave vector of electrons in the xy plane parallel to the surface which is in the $z=0$ plane.

The external potential $\phi_{\text{ext}}(\mathbf{r}, t)$ will give rise to an induced potential. By using linear-response theory to relate the induced potential to the charge-density fluctuation along with Poisson's equation,³¹ it follows that the induced potential outside the medium ($z > 0$) has the form for $z < 0$

$$\phi_{\text{ind}}(\mathbf{r}, t) = \int d^2 \mathbf{q}_{\parallel} \int_{-\infty}^{\infty} d\omega \tilde{\phi}_{\text{ext}}(\mathbf{q}_{\parallel}, \omega) e^{i(\mathbf{q}_{\parallel} \cdot \mathbf{r}_{\parallel} - \omega t)} g(q_{\parallel}, \omega) e^{-q_{\parallel} z}. \quad (5)$$

In this notation, $g(q_{\parallel}, \omega)$ defines the surface response function. Here, it has been implicitly assumed that the external potential ϕ_{ext} is so weak that the medium responds linearly to it. The function $g(q_{\parallel}, \omega)$ is itself related to the density-density response function χ by

$$g(q_{\parallel}, \omega) = \frac{2\pi e^2}{q_{\parallel}} \int_0^{\infty} dz \int_0^{\infty} dz' e^{q_{\parallel}(z+z')} \chi(z, z'; q_{\parallel}, \omega) \equiv - \int_{-\infty}^0 dz e^{q_{\parallel} z} \rho_{\text{ind}}(z; q_{\parallel}, \omega), \quad (6)$$

where the second equality defines the induced surface charge density.

The quantity $\Im m(g)$ is related to the energy absorption in the semiconductor due to the electronic excitations induced by the evanescent external potential. The power absorption is obtained by integrating the Poynting vector over the surface and over time. This gives (see Appendix A of Ref. 28)

$$\Delta E = \frac{1}{4\pi} \int d^2 \mathbf{x}_{\parallel} \int_{-\infty}^{\infty} dt \left(\phi \frac{\partial}{\partial t} \frac{\partial}{\partial z} \phi \right) \Big|_{z=0}, \quad (7)$$

where $\phi = \phi_{\text{ind}} + \phi_{\text{ext}}$ is the total potential with

$$\phi(\mathbf{r}, t) = \int d^2 \mathbf{q}_{\parallel} \int_{-\infty}^{\infty} d\omega [e^{q_{\parallel} z} - g(q_{\parallel}, \omega) e^{-q_{\parallel} z}] e^{i(\mathbf{q}_{\parallel} \cdot \mathbf{x}_{\parallel} - \omega t)} \tilde{\phi}_{\text{ext}}(\mathbf{q}_{\parallel}, \omega). \quad (8)$$

Substituting ϕ into the expression for ΔE in Eq. (7), we obtain after some algebra to the leading order of g

$$\Delta E = \frac{(Ze)^2}{4\pi^2} \int d^2 \mathbf{q}_{\parallel} \int_{-\infty}^{\infty} d\omega \frac{\omega}{q_{\parallel}} (g(q_{\parallel}, \omega))^2 \Im m[g(q_{\parallel}, \omega)]. \quad (9)$$

We now turn to the calculation of the surface response function for a pair of parallel 2DEG layers. In order to make our results appear transparent, we present our transfer-matrix method first for the nonmodulated system. Then, we modify our formalism to include the effects due to a 1D periodic modulation. In this way, we are in a position to compare the results for the plasmon excitations in the presence and absence of a 1D periodic modulation, as well as the absorption spectrum in these two cases. The dispersion equation for a bilayer system without the 1D modulation is well known and has been examined in great detail, following the work of Das Sarma and Madhukar³² as well as that of Santoro and Giuliani.³³

III. SURFACE RESPONSE FUNCTION FOR A BIPLANE

Let us first consider the following device structure. Here, two 2DEG layers are located at $z=0$ and $z=a$ with a slab medium of local dielectric constant $\epsilon(\omega)$ between them and ϵ_r is the background dielectric constant for $z < 0$ and $z > a$. In the nonretarded limit, we take the induced electrostatic potential in the ‘‘vicinity’’ of the $z=0$ layer to be

$$\begin{aligned} \phi_{<}(z) &= e^{-q_{\parallel} z} - g(q_{\parallel}, \omega) e^{q_{\parallel} z}, \quad z \sim 0, \\ \phi_0(z) &= a_0 e^{q_{\parallel} z} + b_0 e^{-q_{\parallel} z}, \quad z = 0^+, \\ \phi_{0>}(z) &= t_0 e^{-q_{\parallel} z} + r_0 e^{q_{\parallel} z}, \quad 0 < z < a, \end{aligned} \quad (10)$$

where all the coefficients are independent of z . Here, we must separate the solutions at the interface since the 2DEG is

embedded within a dielectric medium.²⁷ Both ϕ and $\epsilon d\phi/dz$ must satisfy

$$\phi|_+ - \phi|_- = 0 \quad \text{and} \quad \epsilon_+ \frac{d\phi}{dz} \Big|_+ - \epsilon_- \frac{d\phi}{dz} \Big|_- = 4\pi\sigma_0 \quad (11)$$

across the lower interface layer, where σ_0 is the induced surface charge density in the 2DEG layer at $z=0$. At the upper interface $z=a$, the induced potential is given by

$$\phi_1(z) = a_1 e^{q_{\parallel} z} + b_1 e^{-q_{\parallel} z}, \quad z \sim a, \\ \phi_{1>}(z) = t_1 e^{-q_{\parallel} z}, \quad z > a, \quad (12)$$

where the coefficients a_1, b_1 , and t_1 are determined from the continuity equations for the potential and electric field such

as Eq. (11) with the induced surface charge at $z=a$ denoted by σ_1 . In general, we get $\sigma = \chi_{2D} \phi$ from linear-response theory, where χ_{2D} is the sheet susceptibility, so that $\sigma_0 = \chi_{2D} \phi_0 = (1-g)\chi_{2D}$ and $\sigma_1 = \chi_{2D} \phi(z=a)$. After some algebra, we obtain the coefficients of the potential as given by

$$\vec{\mathbf{A}} \begin{bmatrix} 1-g \\ a_0 \\ b_0 \\ r_0 \\ t_0 \\ a_1 \\ b_1 \\ t_1 \end{bmatrix} = -2 \begin{bmatrix} 0 \\ 1 \\ 0 \\ 0 \\ 0 \\ 0 \\ 0 \\ 0 \end{bmatrix}, \quad (13)$$

where the invertible transfer matrix is

$$\vec{\mathbf{A}} = \begin{bmatrix} 1 & -1 & -1 & 0 & 0 & 0 & 0 & 0 & 0 \\ -\left(\epsilon_r + \frac{4\pi\chi_{2D}}{\epsilon_r q_{\parallel}}\right) & 1 & -1 & 0 & 0 & 0 & 0 & 0 & 0 \\ 0 & 1 & 1 & -1 & -1 & 0 & 0 & 0 & 0 \\ 0 & \epsilon_r & -\epsilon_r & \epsilon(\omega) & -\epsilon(\omega) & 0 & 0 & 0 & 0 \\ 0 & 0 & 0 & e^{-q_{\parallel} a} & e^{q_{\parallel} a} & -e^{q_{\parallel} a} & -e^{-q_{\parallel} a} & 0 & 0 \\ 0 & 0 & 0 & -\epsilon(\omega)e^{-q_{\parallel} a} & \epsilon(\omega)e^{q_{\parallel} a} & -\epsilon_r e^{q_{\parallel} a} & \epsilon_r e^{-q_{\parallel} a} & 0 & 0 \\ 0 & 0 & 0 & 0 & 0 & e^{q_{\parallel} a} & e^{-q_{\parallel} a} & -e^{-q_{\parallel} a} & 0 \\ 0 & 0 & 0 & 0 & 0 & \left(\epsilon_r + \frac{4\pi\chi_{2D}}{\epsilon_r q_{\parallel}}\right) e^{q_{\parallel} a} & \left(-\epsilon_r + \frac{4\pi\chi_{2D}}{\epsilon_r q_{\parallel}}\right) e^{-q_{\parallel} a} & e^{-q_{\parallel} a} & 0 \end{bmatrix}. \quad (14)$$

Equation (13) has the explicit solution for g in terms of the sheet susceptibility as

$$g(q_{\parallel}, \omega) = 1 - 2 \frac{\left[\epsilon(\omega) + \epsilon_r + \frac{4\pi\chi_{2D}}{\epsilon_r q_{\parallel}} \right] + \left[\epsilon(\omega) - \epsilon_r - \frac{4\pi\chi_{2D}}{\epsilon_r q_{\parallel}} \right] e^{-2q_{\parallel} a}}{\left[\epsilon(\omega) + \epsilon_r + \frac{4\pi\chi_{2D}}{\epsilon_r q_{\parallel}} \right]^2 - \left[\epsilon(\omega) - \epsilon_r - \frac{4\pi\chi_{2D}}{\epsilon_r q_{\parallel}} \right]^2 e^{-2q_{\parallel} a}}. \quad (15)$$

The normal modes are obtained by setting the denominator to zero, i.e.,

$$\epsilon_r + \frac{4\pi\chi_{2D}}{\epsilon_r q_{\parallel}} = \epsilon(\omega) \left(\frac{e^{-q_{\parallel} a} \pm 1}{e^{-q_{\parallel} a} \mp 1} \right). \quad (16)$$

In the limit $q_{\parallel} a \rightarrow \infty$, we obtain the surface response for a single plane as

$$g_{\text{single plane}}(q_{\parallel}, \omega) = 1 - \frac{2}{\epsilon_r + \epsilon(\omega) + \frac{4\pi\chi_{2D}}{\epsilon_r q_{\parallel}}}, \quad (17)$$

which was previously derived by Persson.²¹

If we set $\chi_{2D}=0$ in Eq. (15), we obtain the surface response function for a slab of conductive material as

$$g_{\text{slab}}(q_{\parallel}, \omega) = \frac{2 \sinh(q_{\parallel} a)}{\left[\frac{\epsilon(\omega) + \epsilon_r}{\epsilon(\omega) - \epsilon_r} \right] e^{q_{\parallel} a} - \left[\frac{\epsilon(\omega) - \epsilon_r}{\epsilon(\omega) + \epsilon_r} \right] e^{-q_{\parallel} a}} = 2\gamma(q_{\parallel}, \omega) \\ \times \left[\frac{\epsilon(\omega) - \epsilon_r}{\epsilon(\omega) + \epsilon_r} \right] e^{-q_{\parallel} a} \sinh(q_{\parallel} a), \quad (18)$$

where

$$\gamma(q_{\parallel}, \omega) \equiv \left\{ 1 - \left[\frac{\epsilon(\omega) - \epsilon_r}{\epsilon(\omega) + \epsilon_r} \right]^2 e^{-2q_{\parallel} a} \right\}^{-1}. \quad (19)$$

In the limit $a \rightarrow \infty$ for the single interface of a semi-infinite medium, Eq. (18) becomes

$$g_{\text{semi}}(q_{\parallel}, \omega) = \frac{\epsilon(\omega) - \epsilon_r}{\epsilon(\omega) + \epsilon_r}. \quad (20)$$

Let us now set $\epsilon(\omega) = \epsilon_r$ for a dielectric slab and use the approximation³⁴

$$\chi_{2\text{D}}(q_{\parallel}, \omega) \approx -\frac{n_{2\text{D}}e^2q_{\parallel}^2}{m^*(\omega^2 - \beta_{2\text{D}}^2q_{\parallel}^2)} \quad (21)$$

for the 2DEG with electron effective mass m^* and sheet density $n_{2\text{D}}$ in Eq. (21). Here, $\beta_{2\text{D}}^2 = 3v_{\text{F},2\text{D}}^2/8$. By taking $v_{\text{F}}/c \rightarrow 0$ for moderate electron densities, we obtain the dispersion relation for plasmons in the long-wavelength limit as

$$\omega_{\pm}^2 = \omega_{2\text{D}}^2(1 + e^{-q_{\parallel}a}) \quad (22)$$

and

$$\omega_{\pm}^2 = \omega_{2\text{D}}^2(1 - e^{-q_{\parallel}a}), \quad (23)$$

corresponding to a symmetric and an antisymmetric mode. In this notation, $\omega_{2\text{D}} = \sqrt{2\pi n_{2\text{D}}e^2/m^* \epsilon_r}$ is the well-known 2D plasmon frequency. When $q_{\parallel}a \ll 1$, the ω_{+} mode behaves like a 2D plasmon, whereas the ω_{-} mode has the character of an acoustic mode. Also, if we take

$$\epsilon(\omega) = \epsilon_r \left(1 - \frac{\omega_p^2}{\omega^2}\right) \quad (24)$$

for a conductive slab, we obtain the frequency of the coupled 2D plasmon mode interacting with the 3D plasmon. The results are

$$\omega_{\pm}^2 = \omega_{2\text{D}}^2(1 + e^{-q_{\parallel}a}) + \omega_s^2(1 - e^{-q_{\parallel}a}) \quad (25)$$

and

$$\omega_{\pm}^2 = \omega_{2\text{D}}^2(1 - e^{-q_{\parallel}a}) + \omega_s^2(1 + e^{-q_{\parallel}a}), \quad (26)$$

where $\omega_s = \omega_p/\sqrt{2}$ is the surface plasmon frequency. This shows that the symmetric (antisymmetric) mode for the 2D sheet is coupled to the antisymmetric (symmetric) mode of the slab. As a matter of fact, the ω_{-} mode has frequency ω_s and the ω_{+} mode has an effective 2D plasmon frequency for an effective sheet density that includes both the 2D layer and that of the conductive slab.

In addition to the high-frequency modes in Eqs. (25) and (26), there is a low-energy acoustic plasmon mode whose frequency can be obtained analytically in the limit $a \rightarrow \infty$. For this, we keep the $\beta_{2\text{D}}$ in Eq. (21). After a straightforward calculation, we obtain a correction to the results in Eqs. (25) and (26) arising from the nonlocal correction, i.e.,

$$\omega_{\pm}^2 = \omega_{2\text{D}}^2 + \omega_s^2 + \beta_{2\text{D}}^2q_{\parallel}^2, \quad (27)$$

along with

$$\omega_{\text{ac}}^2 = \frac{\omega_s^2\beta_{2\text{D}}^2q_{\parallel}^2}{\omega_{2\text{D}}^2 + \omega_s^2 + \beta_{2\text{D}}^2q_{\parallel}^2}. \quad (28)$$

In the paper by Pitarke *et al.*³⁵ a low-frequency acoustic plasmon mode of the nature of that in Eq. (28) was obtained in addition to the high-frequency plasmon modes we obtained in Eqs. (25)–(27). The reason for the presence of this acoustic plasmon mode for a 2D sheet near the surface of a

semi-infinite metal is due to a nonlocal and dynamically screened Coulomb potential in the dielectric function.

We next consider the effect that a periodic grating on the surface of the material will have on the results derived above. In the presence of the grating, the spatial profile of the x -dependent sheet density can be described as $n_{2\text{D}}(x) = \sum_{n=-\infty}^{\infty} \rho_n \exp(inGx)$, where the real value ρ_n is the n th Fourier component of $n_{2\text{D}}(x)$, $G = 2\pi/d$ is the reciprocal-lattice vector, and d is the period of the grating. In this case, as a generation of Eqs. (10) and (12), the potentials can be expanded by using the Bloch theorem

$$\phi_{<}(\mathbf{r}; \omega) = \sum_{n=-\infty}^{\infty} e^{i(q_x+nG)x} e^{iq_y y} [e^{-q_n z} - g_n(q_x, q_y; \omega) e^{q_n z}], \quad z <$$

$$\sim 0,$$

$$\phi_0(\mathbf{r}; \omega) = \sum_{n=-\infty}^{\infty} e^{i(q_x+nG)x} e^{iq_y y} [a_n(q_x, q_y; \omega) e^{q_n z} + b_n(q_x, q_y; \omega) e^{-q_n z}], \quad z = 0^+,$$

$$\phi_{0>}(\mathbf{r}; \omega) = \sum_{n=-\infty}^{\infty} e^{i(q_x+nG)x} e^{iq_y y} [t_n(q_x, q_y; \omega) e^{-q_n z} + r_n(q_x, q_y; \omega) e^{q_n z}], \quad 0 < z \sim a^-,$$

$$\phi_1(\mathbf{r}; \omega) = \sum_{n=-\infty}^{\infty} e^{i(q_x+nG)x} e^{iq_y y} [a_{1,n}(q_x, q_y; \omega) e^{q_n z} + b_{1,n}(q_x, q_y; \omega) e^{-q_n z}], \quad z \sim a$$

$$\phi_{1>}(\mathbf{r}; \omega) = \sum_{n=-\infty}^{\infty} e^{i(q_x+nG)x} e^{iq_y y} t_{1,n}(q_x, q_y; \omega) e^{-q_n z}, \quad z > a, \quad (29)$$

where $q_n = [q_y^2 + (q_x + nG)^2]^{1/2}$. Furthermore, if the period of the modulation is large with negligible quantum confinement effects, we may approximate the modulated susceptibility by the value for a 2D sheet. Therefore, when $q_x d \rightarrow \infty$, this reduces to the case with an unmodulated 2DEG.

Applying the boundary conditions at $z=0$ to the potential and its derivative, we obtain the following set of linear equations:

$$1 - g_n = a_n + b_n,$$

$$(a_n - b_n + 1 + g_n)q_n = \frac{4\pi}{\epsilon_r} \sum_{n'=-\infty}^{\infty} \chi_{2\text{D}}(q_{n'-n}, \omega) \phi(q_{n'-n})$$

$$= \frac{4\pi}{\epsilon_r} \sum_{n'=-\infty}^{\infty} \chi_{2\text{D}}(q_{n'-n}, \omega) (1 - g_{n'-n}),$$

$$a_n + b_n = t_n + r_n,$$

$$\begin{aligned}
\epsilon_r(a_n - b_n) &= \epsilon(\omega)(-t_n + r_n), \\
t_n e^{-q_n a} + r_n e^{q_n a} &= a_{1,n} e^{q_n a} + b_{1,n} e^{-q_n a}, \\
\epsilon(\omega)(-t_n e^{-q_n a} + r_n e^{q_n a}) &= \epsilon_r(a_{1,n} e^{q_n a} - b_{1,n} e^{-q_n a}), \\
a_{1,n} e^{q_n a} + b_{1,n} e^{-q_n a} &= t_{1,n} e^{-q_n a}, \\
q_n[-t_{1,n} e^{-q_n a} - (a_{1,n} e^{q_n a} - b_{1,n} e^{-q_n a})] &= \frac{4\pi}{\epsilon_r} \sum_{n'=-\infty}^{\infty} \chi_{2D}(q_{n'-n}, \omega) \\
&\times (a_{1,n'-n} e^{q_{n'-n} a} + b_{1,n'-n} e^{-q_{n'-n} a}), \quad (30)
\end{aligned}$$

where $\chi_{2D}(q_n, \omega)$ is given in Eq. (21). These results show that there is a coupling among field components with different reciprocal-lattice vectors. The effect of the modulation on the transmission and reflection coefficients is to couple the lateral degree of freedom to the propagation of the electro-

magnetic wave between the two 2DEGs. Consequently, the energy loss from the structure through the surface response function is *not* determined by its physical properties in one direction only. Assuming a simple sinusoidal form for the sheet density, i.e., $n_{2D}(x) = n_{2D}[1 + \cos(Gx)]/2$, we find non-zero terms of $\chi_{2D}(q_n, \omega)$ only for $n=0, \pm 1$ with $\rho_0 = n_{2D}/2$ and $\rho_{\pm 1} = n_{2D}/4$. However, there are still infinite number of field components with different reciprocal-lattice vectors in this case. In numerical calculations, we have to truncate the number of reciprocal-lattice vectors to a finite value N_0 . The larger the value of N_0 is, the more the plasmon modes can be calculated accurately. As an example, we take $N_0=3$ for $n_{2D}(x) = n_{2D}[1 + \cos(Gx)]/2$. As a result, we will include the coupling between the q_{\parallel} and the $q_{\pm 1} = [q_y^2 + (q_x \pm G)^2]^{1/2}$ modes, then we truncate the set of equations in Eq. (30) to include $n=0, \pm 1$. The resulting 24×24 coefficient matrix for $\{1 - g_n, a_n, b_n, t_n, r_n, a_{1,n}, b_{1,n}, t_{1,n}\}$ with $n=0, \pm 1$ is

$$\vec{\mathbf{M}} = \begin{bmatrix} \vec{\mathbf{M}}_{11}(q_{-1}) & \vec{\mathbf{M}}_{12} & \vec{\mathbf{\Lambda}}(q_{\parallel}) & \vec{\mathbf{0}} & \vec{\mathbf{\Lambda}}(q_1) & \vec{\mathbf{0}} \\ \vec{\mathbf{M}}_{21}(q_{-1}) & \vec{\mathbf{M}}_{22}(q_{-1}) & \vec{\mathbf{0}} & \vec{\mathbf{\Gamma}}(q_{\parallel}) & \vec{\mathbf{0}} & \vec{\mathbf{\Gamma}}(q_1) \\ \vec{\mathbf{\Lambda}}(q_{-1}) & \vec{\mathbf{0}} & \vec{\mathbf{M}}_{33}(q_{\parallel}) & \vec{\mathbf{M}}_{12} & \vec{\mathbf{\Lambda}}(q_1) & \vec{\mathbf{0}} \\ \vec{\mathbf{0}} & \vec{\mathbf{\Gamma}}(q_{-1}) & \vec{\mathbf{M}}_{21}(q_{\parallel}) & \vec{\mathbf{M}}_{22}(q_{\parallel}) + \vec{\mathbf{\Gamma}}(q_{\parallel}) & \vec{\mathbf{0}} & \vec{\mathbf{\Gamma}}(q_1) \\ \vec{\mathbf{\Lambda}}(q_{-1}) & \vec{\mathbf{0}} & \vec{\mathbf{\Lambda}}(q_{\parallel}) & \vec{\mathbf{0}} & \vec{\mathbf{M}}_{11}(q_1) & \vec{\mathbf{M}}_{12} \\ \vec{\mathbf{0}} & \vec{\mathbf{\Gamma}}(q_{-1}) & \vec{\mathbf{0}} & \vec{\mathbf{\Gamma}}(q_{\parallel}) & \vec{\mathbf{M}}_{21}(q_1) & \vec{\mathbf{M}}_{22}(q_1) \end{bmatrix}. \quad (31)$$

In this notation, $\vec{\mathbf{0}}$ is the 4×4 null matrix and $\vec{\mathbf{\Lambda}}$ is a 4×4 submatrix with all its elements equal to zero except the element in the second row and first column with

$$[\vec{\mathbf{\Lambda}}(q_n)]_{21} = -\frac{4\pi\chi_{2D}(q_n, \omega)}{\epsilon_r}. \quad (32)$$

All elements of the 4×4 matrix $\vec{\mathbf{M}}_{12}$ are zero except $[\vec{\mathbf{M}}_{12}]_{31} = -1$ and $[\vec{\mathbf{M}}_{12}]_{41} = \epsilon(\omega)$. Also, $\vec{\mathbf{\Gamma}}$ is a 4×4 submatrix with all its elements equal to zero except the two elements in the fourth row and second and fourth columns with

$$\begin{aligned}
[\vec{\mathbf{\Gamma}}(q_n)]_{42} &= -\frac{4\pi\chi_{2D}(q_n, \omega)}{\epsilon_r} e^{q_n a}, \quad [\vec{\mathbf{\Gamma}}(q_n)]_{43} = \\
&-\frac{4\pi\chi_{2D}(q_n, \omega)}{\epsilon_r} e^{-q_n a}, \quad (33)
\end{aligned}$$

and the only elements of the 4×4 submatrix $\vec{\mathbf{M}}_{21}$ which are nonzero are

$$[\vec{\mathbf{M}}_{21}(q_n)]_{14} = -e^{-q_n a}, \quad [\vec{\mathbf{M}}_{21}(q_n)]_{24} = \epsilon(\omega)e^{-q_n a}. \quad (34)$$

The other 4×4 submatrices $\vec{\mathbf{M}}_{11}$, $\vec{\mathbf{M}}_{22}$, and $\vec{\mathbf{M}}_{33}$ introduced in Eq. (31) are defined as

$$\vec{\mathbf{M}}_{11}(q_n) = \begin{bmatrix} 1 & -1 & -1 & 0 \\ -q_n & q_n & -q_n & 0 \\ 0 & 1 & 1 & -1 \\ 0 & \epsilon_r & -\epsilon_r & \epsilon(\omega) \end{bmatrix}, \quad (35)$$

$$\vec{\mathbf{M}}_{22}(q_n) = \begin{bmatrix} -e^{q_n a} & e^{q_n a} & e^{-q_n a} & 0 \\ -\epsilon(\omega)e^{q_n a} & \epsilon_r e^{q_n a} & -\epsilon_r e^{-q_n a} & 0 \\ 0 & e^{q_n a} & e^{-q_n a} & -e^{-q_n a} \\ 0 & -q_n e^{q_n a} & q_n e^{-q_n a} & -q_n e^{-q_n a} \end{bmatrix}, \quad (36)$$

$$\vec{\mathbf{M}}_{33}(q_{\parallel}) = \begin{bmatrix} 1 & -1 & -1 & 0 \\ -\left\{q_{\parallel} + \frac{4\pi\chi_{2D}(q_{\parallel}, \omega)}{\epsilon_r}\right\} & q_{\parallel} & -q_{\parallel} & 0 \\ 0 & 1 & 1 & -1 \\ 0 & \epsilon_r & -\epsilon_r & \epsilon(\omega) \end{bmatrix}. \quad (37)$$

The frequencies of the normal modes are obtained by solving for the roots of the determinantal equation $\text{Det}[\vec{\mathbf{M}}] = 0$. In the

next section, we numerically calculate the dispersion relation for a pair of 2DEG layers in the presence of a 1D periodic modulation. We examine these modes when their separation is varied. We also analyze the corresponding behavior of the loss function $\Im m(g)$ for a pair of 2DEG layers and compare the results with those obtained when the layer separation is sufficiently large that the coupling between the layers can be neglected. When $a \rightarrow \infty$, the coefficient matrix $\vec{\mathbf{M}}_{\text{single plane}}$ for this case can be obtained from Eq. (31) by forming a 12×12 matrix with the submatrices in the odd-numbered rows and columns. That is,

$$\vec{\mathbf{M}}_{\text{single plane}} = \begin{bmatrix} \vec{\mathbf{M}}_{11}(q_{-1}) & \vec{\Lambda}(q_{\parallel}) & \vec{\Lambda}(q_1) \\ \vec{\Lambda}(q_{-1}) & \vec{\mathbf{M}}_{33}(q_{\parallel}) & \vec{\Lambda}(q_1) \\ \vec{\Lambda}(q_{-1}) & \vec{\Lambda}(q_{\parallel}) & \vec{\mathbf{M}}_{11}(q_1) \end{bmatrix}. \quad (38)$$

We also compute $\Im m(g)$ in the absence of a 1D modulation by using Eqs. (15) and (17) for a bilayer and a single plane, respectively.

IV. NUMERICAL RESULTS

Our dispersion formula for a 2D bilayer in the presence of a modulation potential shows that there is a coupling between the wave-vector components of the response function. This nonlocal effect leads to a splitting of the plasmon modes into branches (band-structure folding), which can be identified with a reciprocal-lattice vector or scattering off a Brillouin-zone boundary. Figures 1 and 2 show plots of our results for the modes of plasmon dispersion with a single layer of 2DEG on the surface of a semi-infinite conductive material ($a \rightarrow \infty$). A 1D sinusoidal modulation in the x direction is present in these calculations. In Figs. 1(a) and 1(b), we plot the scaled plasmon-mode frequencies as a function of $q_x d / \pi$ for $q_y = 0$, $n_{2D} / (n_{3D} d) = 2 \times 10^{-3}$, and $\epsilon_r = 1$. The upper and lower branches in the Fig. 1(a) are associated with the $n = -1$ and $n = 0$ plasmon modes. The effect of the 1D modulation acts to split the degenerate ω_{\pm} modes predicted by either Eq. (25) or (26) with $a \rightarrow \infty$ due to the coupled 2D plasmon interacting with the 1D modulation within the sheet.

The general features found from Fig. 1(a) can be explained as follows. Initially, when $q_x = 0$, the degeneracy between the upper $n = -1$ branch with another $n = 1$ branch above (not shown here) is split by the 1D modulation with a gap proportional to the Fourier component $\rho_0 = n_{2D} / 2$. Therefore, as $q_x d$ increases from zero in the strong coupling regime ($q_x d \ll 1$), the upper $n = -1$ branch is pushed down, exhibiting negative dispersion in the figure. When $q_x d / \pi = 1/2$ is reached, the second degeneracy existing between the upper downward sloping $n = -1$ branch and the lower upward sloping $n = 0$ branch is split again into a smaller gap proportional to the Fourier component $\rho_{+1} = n_{2D} / 4$ of the density modulation. When $q_x d / \pi > 1$ (not shown in the figure), the upper $n = -1$ branch increases with $q_x d$, while the lower $n = 0$ branch decreases as $q_x d$ is increased, creating a symmetrical anticrossing behavior centered at $q_x d / \pi = 1$. When $q_x d / \pi = 2$ is reached, there exists a periodic condition for both the $n = 0$ and $n = -1$ branches due to the periodicity of

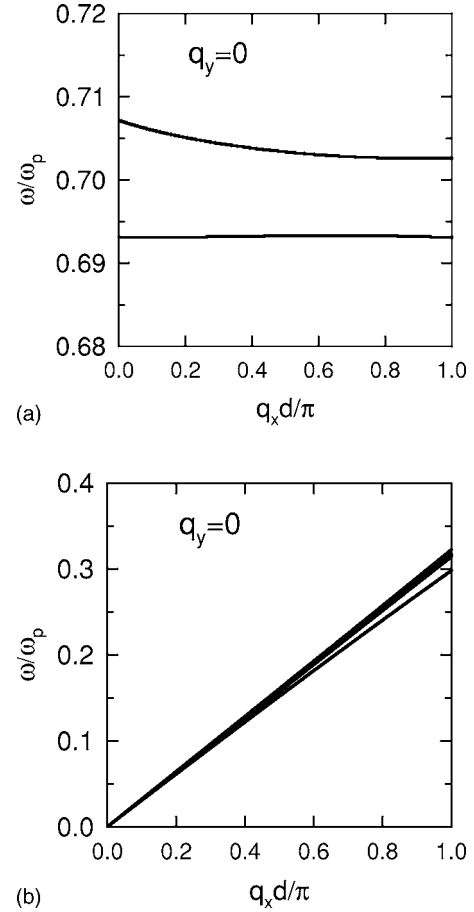


FIG. 1. The plasmon frequencies in units of ω_p , for a single layer of 2DEG in the presence of an electrostatic modulation potential, as a function of $q_x d / \pi$. In (a), only the two lowest modes with finite frequency as $q_x \rightarrow 0$ are shown. In (b), the plasmon spectrum arising from the acoustic mode is displayed. Here, $q_y = 0$, $n_{2D} / n_{3D} d = 2 \times 10^{-3}$, and the parameters used in the calculation are given in the text.

the 1D modulation, i.e., the energies of the $n = -1$ and $n = 0$ modes at $q_x d / \pi = 2$ should have the same value as their initial energies at $q_x = 0$, respectively. As a result, we expect an inversion symmetry of dispersion curves for both the $n = -1$ and $n = 0$ plasmon modes with respect to $q_x d / \pi = 1$.

The modes we plotted in Fig. 1(a) interact weakly with the low-frequency acoustic plasmon mode. This means that they are not significantly affected by the presence of the β_{2D} term in Eq. (22). This is supported by Eq. (27) for the following reason. Typical values of the plasma frequency are $\omega_p \sim 10^{10} - 10^{16} \text{ s}^{-1}$ (See Kittel's book,³⁶ for example). Also, the grating period $d \sim 4 \mu\text{m}$ (Ref. 16) and $v_{F,2D} \approx 4.33 \times 10^3 \text{ m/s}$ for a 2D electron density $n_{2D} = 10^{10} \text{ cm}^{-2}$ and an electron effective mass $m^* = 0.067 m_e$, corresponding to GaAs, where m_e is the free electron mass. Since we are plotting ω / ω_p as a function of $q_x d / \pi$, the scaled frequency of the acoustic plasmon mode is determined by $U = (\pi \beta_{2D} / d \omega_p)^2$. Using the values above for $\omega_p, v_{F,2D}$, and the spacing d , we obtain the values $U \sim 1 - 10^{-12}$ for the range of plasma frequencies. In Fig. 1(b), we chose $U = 0.1$ and plotted the low-frequency region of the plasmon spectrum. The dispersion

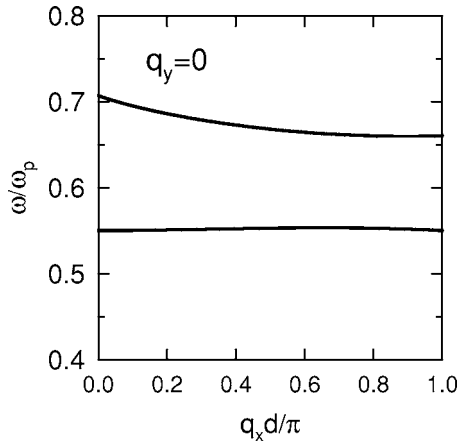


FIG. 2. The same as Fig. 1 except that we chose $n_{2D}/n_{3D}d=2 \times 10^{-2}$.

relation is linear for $q_x \rightarrow 0$. This mode is then split by the presence of the grating as q_x is increased.

Our calculations have shown that the detailed plasmon spectrum depends on the ratio of n_{2D} to $n_{3D}d$. This ratio must be kept sufficiently small so that the lowest plasmon branch will not be suppressed at $q_x=0$. This requires either a large 3D doping or a small sheet density for the fixed grating period. The softening behavior is clearly demonstrated in Fig. 2, where we kept all parameters the same as Fig. 1(a) except that we set $n_{2D}/(n_{3D}d)=10^{-2}$, 1 order of magnitude larger. In this case, both the upper $n=-1$ and lower $n=0$ branches are shifted down in energy due to strong coupling between the 2D plasmon and the 1D modulation, with enhanced gaps at $q_x=0$ and at $q_x d/\pi=1$, for both branches.

Figure 3 displays a plot of the imaginary part of the surface response function $\Im m(g_{-1})$ as a function of ω/ω_p for $q_x=0$ and $q_y d=2$ with a single layer of 2DEG on the surface of a semi-infinite conductive material. In this calculation, we added a small positive imaginary part $\delta=10^{-2}\omega_p$ to the frequency of $g_n(q_x, q_y; \omega)$. Choosing a different value for δ leads to some quantitative differences but the conclusions remain the same. There is a “peak” associated with the lower $n=0$ plasmon branch in Fig. 1 with positive dispersion

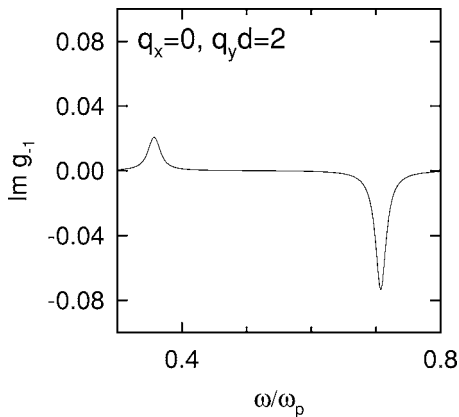


FIG. 3. The imaginary part of g_{-1} as a function of ω/ω_p corresponding to $q_x=0$ and $q_y d=2$. The other parameters are the same as in Fig. 1.

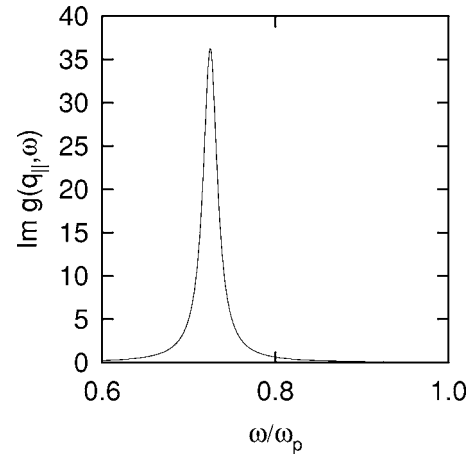


FIG. 4. The imaginary part of g in Eq. (17) as a function of ω/ω_p corresponding to $q_x=0$ and $q_y d=2$ for a 2DEG layer in the absence of an electrostatic modulation. The other parameters are the same as in Fig. 1.

around $q_x=0$, and there is a “dip” associated with the upper $n=-1$ plasmon branch with negative dispersion. The extreme-value frequencies are slightly shifted away from those of the plasmon modes for these wave vectors. The reason is due to the fact that the plasmon resonances were obtained by finding where the determinant of the coefficient matrix $\vec{M}_{\text{single plane}}$ vanishes for real ω . However, the peak or dip in $\Im m(g_{-1})$ occurs when both the real and imaginary parts of the determinant of g_{-1} have their smallest values for complex frequency. As we varied the value of q_x away from zero to $q_x d/\pi=2$, there were ranges of frequency where the dip became a peak and vice versa in the imaginary part of g_{-1} due to switching between negative and positive dispersions in the anticrossing region. Similar behavior was obtained when we plotted the imaginary parts of g_0 and g_1 as functions of ω . However, although the locations of these dips or peaks are similar, their strengths are different. A dip in the surface response function corresponds to a gain in energy, whereas a peak indicates a loss. In Fig. 4, we plot the imaginary part of $g_{\text{single plane}}(q_{||}, \omega)$ given by Eq. (17) in the absence of the 1D modulation as a function of ω/ω_p . The values for q_x , q_y , and ϵ_r are the same as those in Fig. 3. There is just one peak arising from the coupled 2D and 3D surface plasmon excitations, indicating that the dip seen in Fig. 3 comes from the 1D modulation to the 2DEG layer or the plasmon-mode ($n=\pm 1$) splitting at $q_x=0$.

We now present our numerical calculations for a pair of 2DEG layers (finite a) interacting with 3D electrons. In Fig. 5, we plot the plasmon dispersion relation as a function of $q_x d/\pi$ when $a/d=1.5$, $q_y d=2$, $n_{2D}/(n_{3D}d)=10^{-3}$, and $\epsilon_r=1$. The upper and lower branches in Fig. 1 are split respectively into a pair (ω_+/ω_- modes), as predicted by Eqs. (25) and (26) through the interaction of two conducting surfaces separated by a distance a . The upper and lower pairs around $q_x=0$ correspond to $n=-1$ and $n=0$, noting that $\omega_s/\omega_p=1/\sqrt{2} \approx 0.7$. For this case, the second terms of Eqs. (25) and (26) dominate the first terms. The upper plasmon mode (ω_+ mode for the $n=-1$ pair and ω_- mode for the $n=0$ pair) of each pair always has a negative dispersion around $q_x=0$, while the

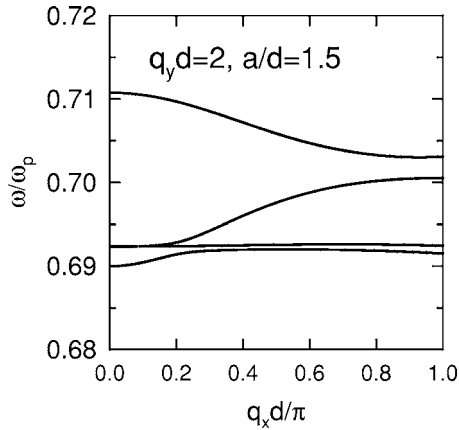


FIG. 5. Plot of the lowest plasmon frequencies in units of ω_p , for a pair of 2DEG layers with separation $a=1.5d$, as a function of $q_x d/\pi$. We chose $n_{2D}/n_{3D}d=2 \times 10^{-2}$. The parameters used in the calculation are given in the text.

lower plasmon mode (ω_- mode for the $n=-1$ pair and ω_+ mode for the $n=0$ pair) of each pair has a positive dispersion. The second and the third plasmon modes (ω_- modes for the $n=0$ and $n=-1$ pairs) counted from the bottom almost have the same energy (close to the surface plasmon energy $\hbar\omega_s$) around $q_x=0$ due to $q_y a > 1$ in Eqs. (25) and (26). The interaction between the pair of 2DEG layers is very strong at $q_x=0$ for the upper $n=-1$ pair, leading to a large splitting of ω_+/ω_- modes. However, this interaction is greatly suppressed at $q_x d/\pi=1$, leading to a much smaller splitting of ω_+/ω_- modes for the $n=-1$ pair.

In Figs. 6 and 7, we plot $\Im m(g_{-1})$ from the solution of Eq. (30) and $\Im m[g(q_{\parallel}, \omega)]$ given in Eq. (15), for $q_x=0$ and $q_y d=2$. Both figures display Z-shape feature, i.e., a positive peak is closely followed by a negative dip or vice versa, which arises from the strong electrostatic coupling between two 2DEG layers. We have noted from Fig. 5 that the upper plasmon mode of the $n=0$ pair and the lower plasmon mode of the $n=-1$ pair are almost degenerate with each other when $q_x=0$. For the very sharp Z-shape feature in Fig. 6 within the

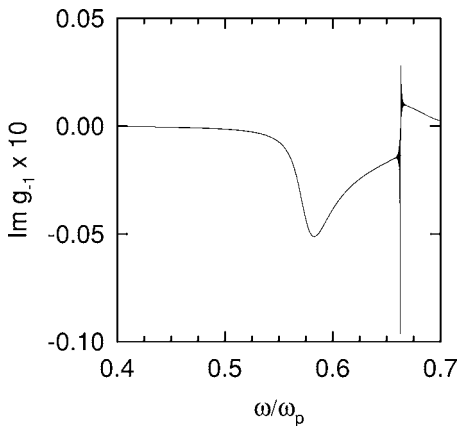


FIG. 6. The imaginary part of g_{-1} as a function of ω/ω_p for $q_x=0$ and $q_y d=2$ for a pair of 2DEG layers in the presence of an electrostatic modulation. The other parameters are the same as in Fig. 5.

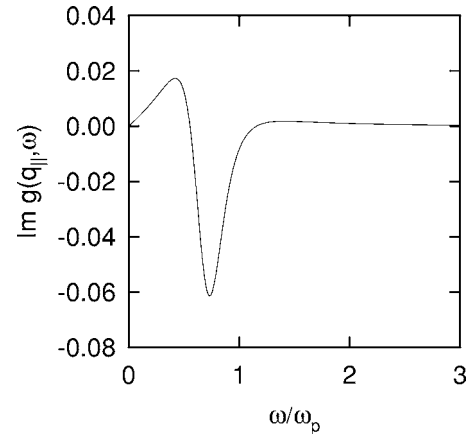


FIG. 7. The imaginary part of g in Eq. (15) as a function of ω/ω_p for $q_x=0$ and $q_y d=2$ for a pair of 2DEG layers in the absence of an electrostatic modulation. The other parameters are the same as in Fig. 5.

range of $0.6 < \omega/\omega_p < 0.7$, it is found to relate to the upper plasmon mode (ω_+ mode) of the $n=-1$ pair. The broadened dip slightly below $\omega/\omega_p=0.6$ comes from the degenerate lower plasmon mode (ω_- mode) of the $n=-1$ pair and the upper plasmon mode (ω_- mode) of the $n=0$ pair. For the smooth Z-shape feature seen in Fig. 7 within the range of $0 < \omega/\omega_p < 1$, the low-energy positive peak is associated with the ω_+ mode, while the high-energy negative dip is associated with the ω_- mode. The crucial difference between these two graphs is that the periodic modulation greatly enhances the dip and the peak. We have also examined the behavior of $\Im m(g_0)$ and $\Im m(g_1)$ and found that their dips and peaks are also enhanced compared with those shown in Fig. 7 for an unmodulated bilayer. The Z-shape feature remained as we varied the wave-vector components q_x and q_y .

V. CONCLUDING REMARKS

We conclude with a discussion of the significance of our results and the potential device applications. We have calculated the plasmon excitation spectrum of a grating-gated double-quantum-well field-effect transistor structure with the help of the surface response function. We restricted our attention to the low-temperature electric quantum limit where only one subband of the 2DEG is occupied. If the electron density is such that higher subbands are to be included, then the boundary conditions at the heterointerface must be modified. The new boundary conditions should include the finite thickness of the electron gas layers. In addition, the dielectric-response function for the interface electrons need to account for multisubband and finite temperature effects.

It was shown that the essential characteristics of the response are multiple plasmon resonances corresponding to spatial harmonics of standing waves in the gap regions of a metal grating. This is due to the static spatial modulation of the electron density in the 2DEG layers. We have compared our results for the loss function with the bilayer structure un gated. It is known that the plasmon modes may radiate energy for a pair of coupled layers of 2DEG.¹⁻³ This has

been demonstrated in our calculated loss function by negative dips. The two-dimensional plasmon modes become more responsive as the doping of the adjoining 3D material is increased and the period of the split-gated modulation is decreased in the strong coupling regime. This is consistent with the experiments aimed at combining the tunability of the grating-gated detector with its high responsivity. The radiation of energy by plasmon modes occurs when these modes become unstable. If a current beam passes in the vicinity of the surface, the 2D plasmon modes in adjacent layers absorb energy for their excitation. However, due to their mutual interaction, these self-sustaining oscillations exist only for a

finite length of time. The damping of these modes results in their excitation energy being radiated from the plasma.

ACKNOWLEDGMENTS

We acknowledge partial support from the National Science Foundation under Grants No. DMR-0303574 and No. CREST 0206162, PSC-CUNY Grant No. 68387-00-37 as well as Grant No. P120A050057-06 from the U.S. Department of Education, and the partial support from the Air Force Office of Scientific Research (AFOSR).

-
- ¹P. Bakshi, J. Cen, and K. Kempa, *J. Appl. Phys.* **64**, 2243 (1988).
²J. Cen, K. Kempa, and P. Bakshi, *Phys. Rev. B* **38**, 10051 (1988).
³K. Kempa, P. Bakshi, J. Cen, and H. Xie, *Phys. Rev. B* **43**, 9273 (1991).
⁴X. G. Peralta, S. J. Allen, M. C. Wanke, N. E. Harff, J. A. Simmons, M. P. Lilly, J. L. Reno, P. J. Burke, and J. P. Eisenstein, *Appl. Phys. Lett.* **81**, 1627 (2002).
⁵V. V. Popov, O. V. Polischuk, T. V. Teperik, X. G. Peralta, S. J. Allen, N. J. M. Horing, and M. C. Wanke *J. Appl. Phys.* **94**, 3556 (2003).
⁶S. Katayama, *J. Phys. Soc. Jpn.* **60**, 1123 (1991).
⁷R. J. Wilkinson *et al.*, *J. Appl. Phys.* **71**, 6049 (1992).
⁸S. Katayama, *Surf. Sci.* **263**, 359 (1992).
⁹W. L. Schaich, P. W. Park, and A. H. MacDonald, *Phys. Rev. B* **46**, 12643 (1992).
¹⁰C. Steinebach, D. Heitmann, and V. Gudmundsson, *Phys. Rev. B* **56**, 6742 (1997).
¹¹S. A. Mikhailov, *Phys. Rev. B* **58**, 1517 (1998).
¹²B. P. van Zyl and E. Zaremba, *Phys. Rev. B* **59**, 2079 (1999).
¹³V. V. Popov, T. V. Teperik, O. V. Polischuk, X. G. Peralta, S. J. Allen, N. J. M. Horing, and M. C. Wanke, *Phys. Solid State* **46**, 153 (2004).
¹⁴G. Lenz, R. Parker, M. C. Wanke, and C. M. De Sterke, *Opt. Commun.* **218**, 87 (2003).
¹⁵E. A. Shaner, Mark Lee, M. C. Wanke, A. D. Grine, J. L. Reno, and S. J. Allen, *Proc. SPIE* **6120**, 612006 (2006).
¹⁶Eric A. Shaner, Michael C. Wanke, Mark Lee, John L. Reno, S. J. Allen, and Xomalin G. Peralta, *Proc. SPIE* **5790**, 116 (2005).
¹⁷D. L. Mills and A. A. Maradudin, *Phys. Rev. B* **12**, 2943 (1975).
¹⁸J. Moreland, A. Adams, and P. K. Hansma, *Phys. Rev. B* **25**, 2297 (1982); A. Adams, J. Moreland, P. K. Hansma, and Z. Schlesinger, *ibid.* **25**, 3457 (1982).
¹⁹J. C. Tsang, J. R. Kirtley, and T. N. Theis, *Solid State Commun.* **35**, 667 (1980).
²⁰E. Zaremba, I. Nagy, and P. M. Echenique, *Phys. Rev. B* **71**, 125323 (2005).
²¹B. N. J. Persson, *Solid State Commun.* **52**, 811 (1984).
²²B. N. J. Persson, *Surf. Sci.* **92**, 265 (1980).
²³G. Gumbs, *Phys. Rev. B* **37**, 10184 (1988).
²⁴G. Gumbs, *Solid State Commun.* **65**, 393 (1988).
²⁵G. Gumbs, in *Interfaces, Quantum Wells, and Superlattices*, NATO Advanced Study Institute, Series B: Physics, edited by C. R. Leavens and R. Taylor (Plenum, New York, 1988), P. 153.
²⁶You-Nian Wang and Z. L. Misković *Phys. Rev. A* **66**, 042904 (2002).
²⁷B. N. J. Persson and J. E. Demuth, *Phys. Rev. B* **30**, 5968 (1984); **42**, 8057 (1990).
²⁸A. Liebsch, *Phys. Rev. B* **36**, 7378 (1987).
²⁹H. Ibach and D. L. Mills, *Electron Energy Loss Spectroscopy and Surface Vibrations* (Academic, New York, 1982).
³⁰Godfrey Gumbs, *Phys. Rev. B* **39**, 5186 (1989).
³¹B. N. J. Persson and E. Zaremba, *Phys. Rev. B* **31**, 1863 (1985).
³²S. Das Sarma and A. Madhukar, *Phys. Rev. B* **23**, 805 (1981).
³³G. E. Santoro and G. F. Giuliani, *Phys. Rev. B* **37**, 937 (1981).
³⁴J. K. Jain and P. B. Allen, *Phys. Rev. Lett.* **54**, 2437 (1985).
³⁵J. M. Pitarke, V. U. Nazarov, V. M. Silkin, E. V. Chulkov, E. Zaremba, and P. M. Echenique, *Phys. Rev. B* **70**, 205403 (2004).
³⁶C. Kittel, *Introduction to Solid State Physics*, 6th ed. (Wiley, New York, 1986), p. 258.